NANO LETTERS

Letter

pubs.acs.org/NanoLett

Three-Dimensional Tracking and Visualization of Hundreds of Pt−Co Fuel Cell Nanocatalysts During Electrochemical Aging

Yingchao Yu,[†,∥] Huolin L. Xin,[‡,∥,#] Robert Hovden,[§,⊥] Deli Wang,[†] Eric D. Rus,[†] Julia A. Mundy,[§] David A. Muller,*[,§,⊥] and Héctor D. Abruña*[,†]

[†]Department of Chemistry and Chemical Biology and [‡]Department of Physics, Cornell University, Ithaca, New York 14853, United States

[§]School of Applied and Engineering Physics and [⊥]Kavli Institute, Cornell University, Ithaca, New York 14853, United States

Supporting Information

ABSTRACT: We present an electron tomography method that allows for the identification of hundreds of electrocatalyst nanoparticles with one-to-one correspondence before and after electrochemical aging. This method allows us to track, in three-dimensions, the trajectories and morphologies of each Pt−Co nanocatalyst on a fuel cell carbon support. In conjunction with the use of atomic-scale electron energy loss spectroscopic imaging, our experiment enables the correlation of performance degradation of the catalyst with changes in particle/interparticle morphologies, particle−support interactions, and the near-surface chemical composition. We found that aging of the catalysts under normal fuel cell operating conditions (potential scans from +0.6 to +1.0 V for 30 000 cycles) gives rise to coarsening of the nanoparticles, mainly through coalescence, which in turn leads to the loss of performance. The observed coalescence events were found to be the result of nanoparticle migration on the carbon support during potential cycling. This method provides detailed insights into how nanocatalyst degradation occurs in proton exchange membrane fuel cells (PEMFCs) and suggests that minimization of particle movement can potentially slow down the coarsening of the particles and the corresponding performance degradation.

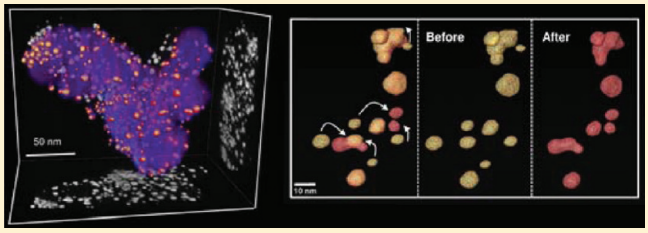

KEYWORDS: *Tomography, electrocatalysis, STEM, fuel cell, ORR, EELS*

Proton exchange membrane fuel cells (PEMFCs) represent an attractive energy conversion technology, which is also an environmentally friendly alternative to the internal combustion engine used in automobiles.[1,2] In a PEMFC, hydrogen fuel is oxidized at the anode and oxygen is reduced at the cathode to produce water and electricity. While the standard reduction potential of O_2 to H_2O is +1.23 V, the kinetics of the oxygen reduction reaction (ORR) are notoriously slow, giving rise to large overpotentials. As a result, much recent work has focused on the improvement of the cathode's electrocatalytic activity by synthesizing nanoparticles composed of platinum alloyed with a second element.[3−6] Among these, one of the most promising candidates is Pt_3Co, which has been shown both experimentally[7] and theoretically[8] to have a 2−4 fold enhancement in the ORR kinetics relative to pure Pt. However, the rapid degradation of the Pt_3Co nanocatalyst results in unacceptably short life times of the fuel cell.[1] To date, the cost and degradation of cathode catalyst are two of the major barriers for the commercialization of PEMFCs. Therefore, it is of great importance to understand the degradation mechanisms of the nanocatalyst particles during electrochemical aging in a fuel cell cathode. A great deal of past efforts have focused on the ex situ study of the nanocatalyst after electrochemical aging in a membrane electrode assembly (MEA, the electrochemical interface of a fuel cell).[9−11] In these experiments, the MEA was sectioned for TEM analysis, making repeated observations on the same particles impossible. Consequently, particle trajectories were not available, making it difficult to unravel the concurrent coarsening effects of particle coalescence and Ostwald ripening.[9−13] In addition, particle-support interactions are also of great importance to the coarsening of the nanoparticles.[14−16] However, with two-dimensional (2D) images alone, one cannot determine how the catalyst particles are distributed on a three-dimensional (3D) fuel cell carbon support.[17−20]

Herein, we present a 3D tomographic method that allows us to track, in 3D, the trajectories and morphological changes of individual Pt−Co nanocatalyst particles on a fuel cell carbon support, before and after electrochemical aging via potential sweeps. To achieve this, we carried out the electrochemical experiments directly on a TEM support grid.[21−24] In essence, a carbon-coated gold index grid was used as the working electrode in a three electrode electrochemical cell (Figure 1a). The fuel cell catalyst materials were deposited on the grid prior to the electrochemical experiments. The grid (Figure 1b) contained indexed windows, allowing us to perform electron tomography on exactly the same region of the catalyst material before (Figure 1c) and after (Figure 1d) aging, from which we

Received: November 8, 2011
Revised: December 20, 2011
Published: December 27, 2011

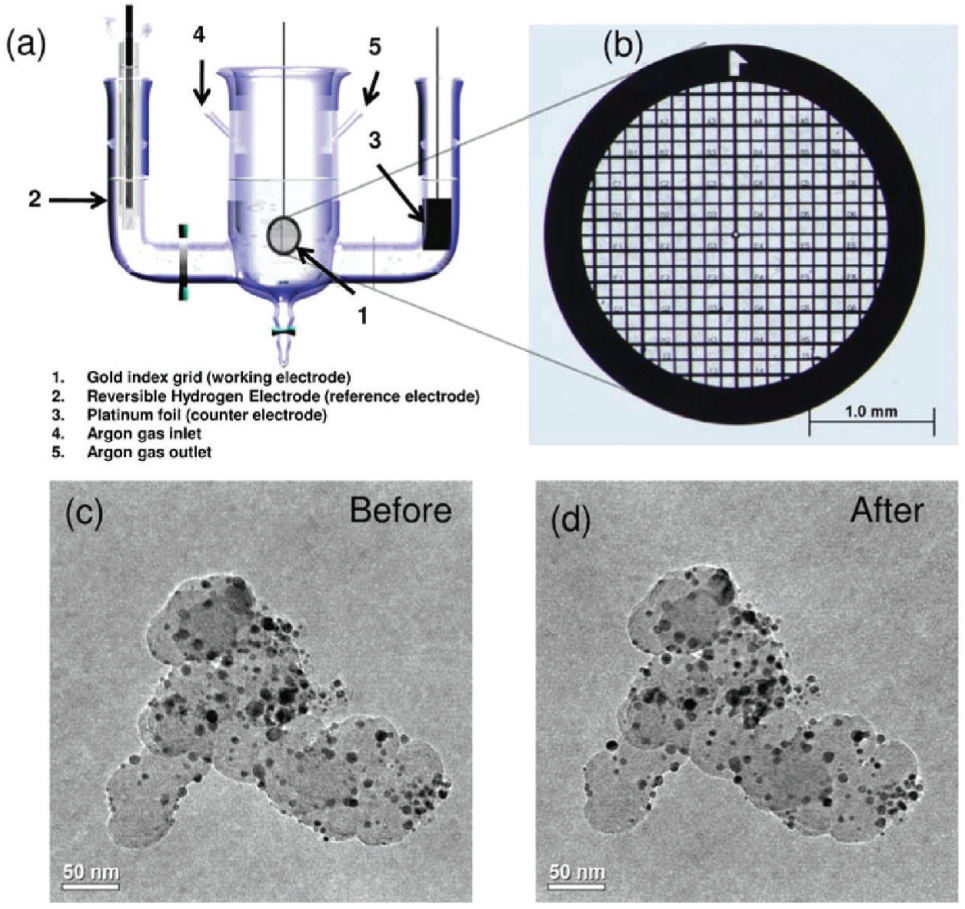

Figure 1. (a) Schematic of the three electrode electrochemical cell. (b) The carbon-coated gold finder grid. (c,d) Bright-field TEM images of the same Pt−Co fuel cell material (metallic nanocatalyst loaded on 3D carbon-black supports) identified before (c) and after (d) electrochemical aging.

were able to identify hundreds of nanoparticles in 3D with precise one-to-one correspondence. This enabled us to study the coarsening evolution of the particles by tracking location changes on the support surface, observing changes in particle volume, and directly visualizing coarsening events. We found that following extensive cycling of the Pt−Co catalysts under normal fuel cell operating conditions (potential scan from +0.6 to +1.0 V for 30 000 cycles), the coarsening could be mainly attributed to coalescence of the nanoparticles. Furthermore, the observed coalescence and movement of the nanocatalyst particles was found not to be the result of carbon support degradation within our experimental resolution of 0.5−1.0 nm. In addition, in order to detect changes in the near-surface composition of the catalysts, we also performed atomic-scale electron energy loss spectroscopic (EELS) imaging of the nanoparticles from which we extracted the chemical composition of the near-surface volume of the particles after potential cycling.

In our study, a carbon-coated gold TEM grid with indexed windows (Figure 1b) was chosen as the working electrode. The indexed windows facilitated the determination of locations of the same catalyst materials before and after the electrochemical aging (Figure 1c) in a three-compartment electrochemical cell (Figure 1a). Gold grids were chosen because they are relatively inert over the potential range of interest. To demonstrate that the TEM grid is a reliable electrode, we characterized the grid from two aspects. First, Supporting Information Figure 1Sa presents a comparison of the voltammetric profiles of a gold TEM grid and a gold disk electrode. Both profiles exhibited a Au-oxide reduction peak at approximately +1.2 V (vs RHE), which was characteristic of a gold surface. (In the rest of the text, reported potentials are referenced to a RHE unless otherwise specified.) The double-layer region exhibited a capacitive response, which indicated that the surface of the grid was free of contamination. Second, the cross-talk between the catalyst material and the electrode should be minimal under the electrochemical aging conditions of interest, that is, between +0.6 to +1.0 V in our experiments. Supporting Information Figure 1Sb shows that, below +1.4 V, interference from the gold TEM substrate was not significant, demonstrating the electrochemical reliability of the grid. In addition to the cycling setup, it is crucial to choose the appropriate electrochemical aging method. In the case of platinum, previous studies have suggested that potential cycling is more damaging than holding the potential at a given value[25,26] (Supporting Information Figure 2S), and that a triangular waveform is more damaging than a square wave.[27] Therefore, we chose to cycle the potential with a triangular wave, so as to introduce more severe aging effects to the electrocatalyst nanoparticles.

The aging experiment was performed at a scan rate of 50 mV/s, between +0.6 to +1.0 V (vs RHE), and a complete cycle from +0.05 to +1.2 V was carried out immediately after each thousand cycles to determine the electrochemical surface area (ECSA) of the catalyst. The choice of aging window of +0.6 to +1.0 V and 30 000 cycles is based on the U.S. Department of Energy (DOE) accelerated stress test protocols

dx.doi.org/10.1021/nl203920s | *Nano Lett.* 2012, 12, 4417−4423

for PEMFCs.[28] The electrochemical aging results are shown in Figure 2a. Two key changes are highlighted by the blue and red dashed circles. First, the hydrogen adsorption peak at around +0.27 V in the anodic scan became sharper with aging. This sharpening effect was ascribed to the nanocatalyst surfaces becoming more Pt rich. The EELS spectrum analysis further confirmed such an assertion (*vide infra*). Moreover, the hydrogen adsorption peaks at higher potential increased at the expense of those at lower potential. This is typically an indication of exposure of different facets after the electrochemical treatment.[29] The second feature to notice is the shift in the platinum oxide reduction peak at around +0.8 V to more positive values. To exclude the possibility that such a shift was due to the acid-leaching of cobalt, a set of control experiments was carried out on pure Pt nanocatalysts (i.e., no cobalt), as shown in Supporting Information Figure 3S. The results indicate that the positive shift of Pt oxide reduction peak could be observed both in Pt_3Co/C and Pt/C. Consequently, we ascribe the positive shift of the Pt−O reduction peak not due to Co leaching. It was speculated that such shift could be caused by the increase in the size of the nanoparticles, as it has been previously reported that a growth in the size of the nanoparticles is often accompanied by a shift in the Pt−O reduction peak.[30,31] In our study, accompanied by the size increase of some nanoparticles, the overall surface area decreased, as suggested by the ECSA measurements in Figure 2b. The ECSA was calculated by determining the charges associated with the adsorption and desorption of hydrogen between +0.05 and +0.40 V, assuming 0.21 mC/cm^2 as the conversion factor for one monolayer of adsorbed hydrogen. Upon electrochemical aging, platinum was first oxidized to platinum oxide in the anodic scan (with an onset potential around +0.80 V), and the oxide was subsequently reduced back to platinum during the cathodic scan (with a peak potential at around +0.80 V). The dissolution−redeposition process results in a decrease in the ECSA.[32] At the end of the 30 000 cycles, the ECSA had dropped to around 87% of its initial value. This provides a direct indication of the overall changes in the surface area of the nanocatalysts.

The ORR polarization curves on the Pt_3Co/C nanocatalyst, before and after different extents of aging cycles, are shown in Figure 2c,d. The experiments were recorded on the same RDE electrode in an O_2-saturated 0.1 M $HClO_4$ solution at a rotation rate of 1600 rpm after regular intervals of electrochemical aging. Metrics by which the activity of the nanocatalyst toward the ORR can be assessed include the potential at half-maximum kinetic current ($E_{1/2}$), and the current at +0.85 and +0.90 V. The last two can be used to evaluate the mass activity, by normalizing the kinetic current to the mass of the nanocatalyst on the electrode surface (Supporting Information Figure 3S for more detail). We found that the $E_{1/2}$ shifted in the negative

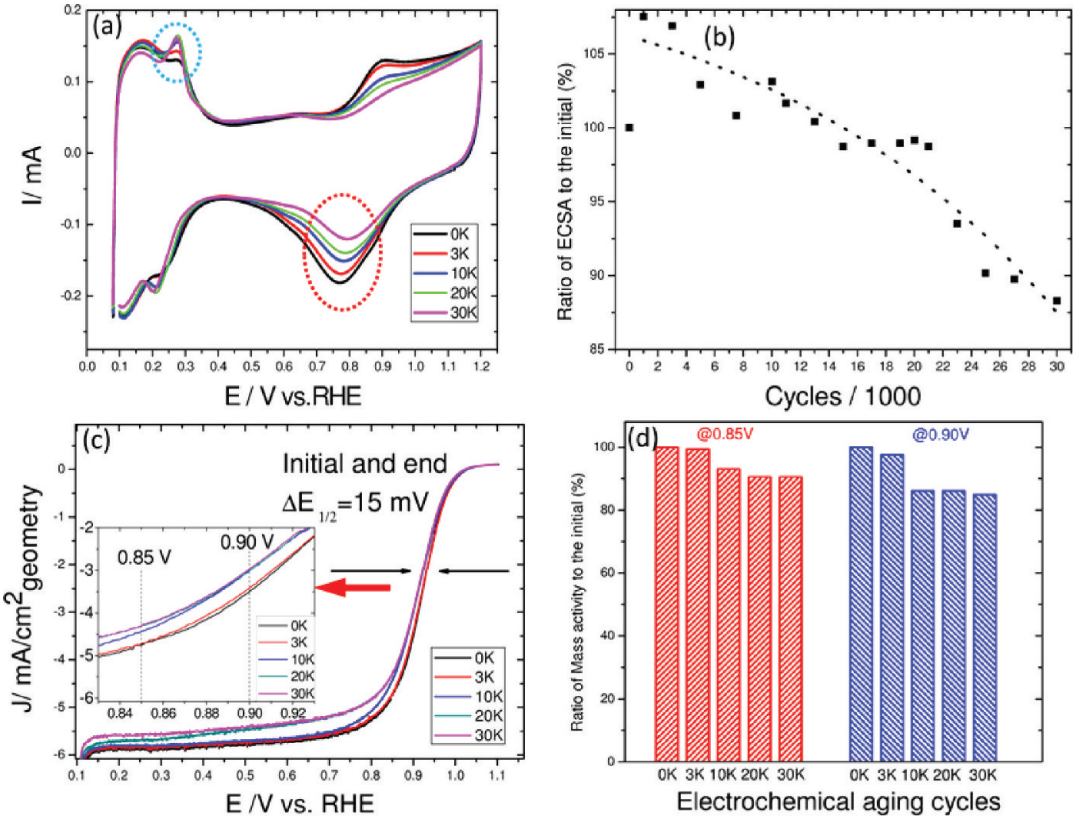

Figure 2. (a) Cyclic voltammogram (CV) of Pt_3Co/C nanocatalyst, before electrochemical aging (0K), and after 3000 (3K, "K" represents 1000), 10K, 20K and 30K cycles (between +0.6 and +1.0 V) in 0.1 M $HClO_4$ at a scan rate of 50 mV/s. The blue dashed-circle highlights the sharpening of the H_2 adsorption peak at ~+0.27 V. The hydrogen adsorption peaks at higher potential increase at the expense of those at lower potential. It is an indication the {100} facets grow at the expense of {111} facets.[29] The red-dashed circle highlights the shift of the Pt−O reduction peak to more positive potentials. (b) Plot of ECSA as a fraction of its initial value and as a function of the number of cycles, for experiments performed on a gold grid. (c) RDE voltammograms of the oxygen reduction reaction (ORR) during the aging process in O_2 saturated 0.1 M $HClO_4$ solution at a scan rate of 5 mV/s and rotating rate of 1600 rpm. Inset is the magnification from +0.83 to +0.93 V. The shift in the potential at half-maximum kinetic current ($\Delta E_{1/2}$) was 15 mV. (d) Percentile of mass activity calculated at +0.85 (red) and +0.90 V (blue) compared to its initial value during the aging process.

dx.doi.org/10.1021/nl203920s | *Nano Lett.* 2012, 12, 4417−4423

direction by about 15 mV and that the mass activity at +0.85 and +0.90 V decreased by 15−20% after 30 000 cycles of aging. Such a loss in ORR activity was consistent with the ECSA results. The degradation of the nanocatalyst was further confirmed by CO stripping (Supporting Information Figure 4S). The CO oxidation peak shifted to lower potentials, suggesting that the aging process resulted in an increase of the effective particle size. By comparing the integrated area of CO oxidation peak (Supporting Information Figure 4S), a 22% surface area loss was also observed, which was in agreement with the ECSA measurement.

Supporting Information Figures 5S−7S present bright-field TEM comparisons of the Pt−Co nanocatalyst materials. Owing to the labeled TEM tracing grid, it was possible to locate the same areas before and after electrochemical aging. It has been reported that carbon corrosion can play an important role in the degradation of Pt-based nanocatalysts in an MEA,[15,16] in which the potential at the cathode could go significantly above +1.0 V, especially under hydrogen starvation conditions, so the carbon support can be oxidized. However, that was not the case in our study. In the three-electrode system employed, control of the potential upper limit during potential cycling was accurate without ambiguity. As evident in the lower-magnification images in Supporting Information Figure 7S, over the cycling range of +0.6 to +1.0 V no large-scale degradation of the carbon support was observed. From the higher-resolution images used for the tomographic series (Supporting Information Figure 6Sc−e), any changes to the support on a scale larger than 0.5−1 nm could be excluded. However, we lack the 3D resolution to detect atomic-scale (i.e., < 0.5 nm) changes on the curved surfaces of the support. Therefore, we cannot rule out the possibility of atomic-scale changes of the support's surface at the particle−support anchoring point. In order to eliminate the possibility that the coarsening may be caused by other effects during the handle of TEM grid, a control experiment (Supporting Information Figure 2S) was performed in which the potential was held constantly at +1.2 V for 16 h after the electrochemical aging. Virtually no change could be observed from both TEM and ECSA measurements. Thus, the coarsening events were attributed to the potential cycling. In Supporting Information Figure 5S, the particles circled in yellow were suspected to have sintered during aging.

To further explore their chemical compositions, EELS mapping of those 17 spots after electrochemical aging was performed and the results are present in Figure 3 (the detailed methods of the EELS mapping can be found elsewhere[12,33−35]). A Pt-rich shell was clearly observed with an average shell thickness determined to be 0.85 ± 0.04 nm for single-core nanoparticles and 0.93 ± 0.07 nm for multicore nanoparticles. Both numbers correspond to a Pt shell thickness of 3−4 Pt monolayers (see Supporting Information Figure 8S for more details on determining the Pt shell thickness). This final shell thickness is less

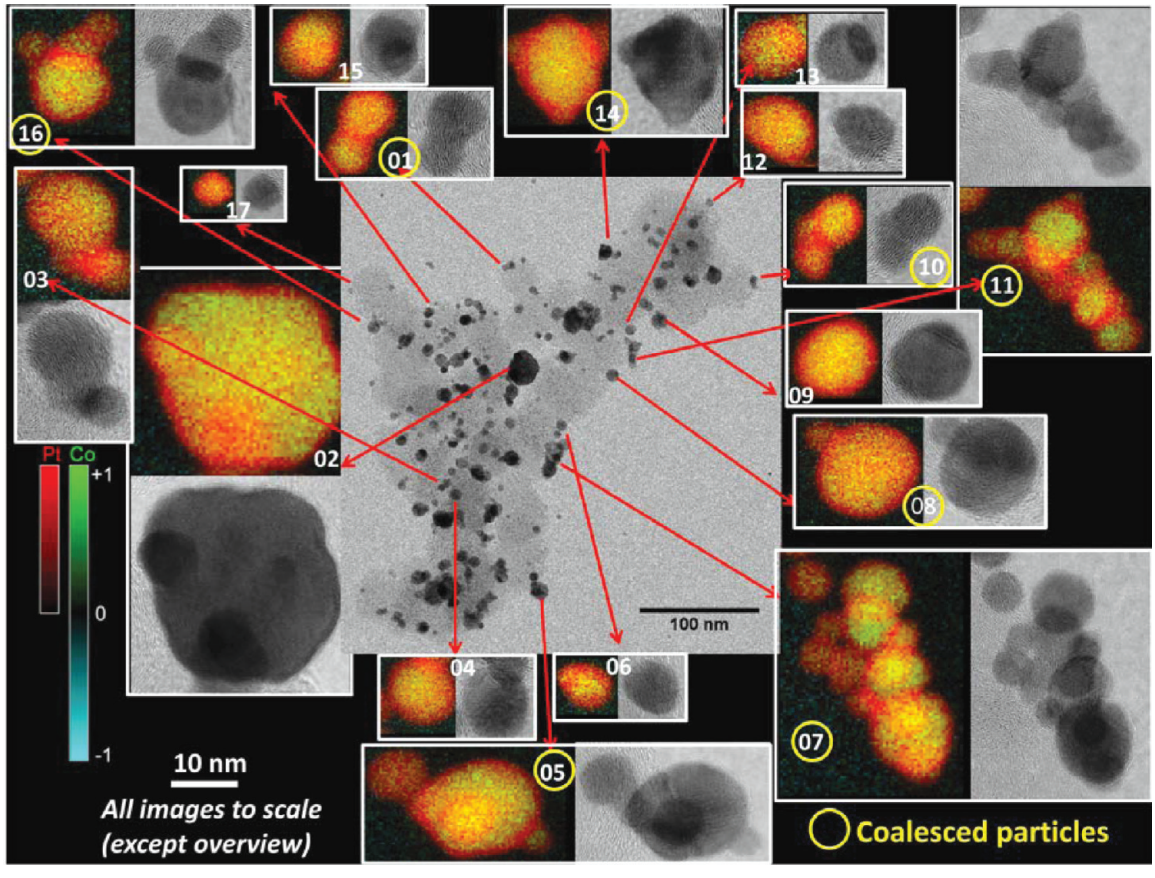

Figure 3. Pt_3Co/C nanocatalyst after electrochemical aging. The overall bright-field transmission electron microscopy image is shown in the center, with specific areas highlighted alongside Pt/Co chemical maps obtained by EELS. The relative Pt concentration is shown in red and the Co concentration in green; yellow indicates a PtCo alloy. The arrow on the EELS map points out the position of the targeted particle from its carbon support. The yellow circle on the number indicates particles that were coalesced. All images (except the overview) are to the same scale for easy comparison.

dx.doi.org/10.1021/nl203920s | *Nano Lett.* 2012, 12, 4417−4423

than the values in our previous study of the same starting material where the Pt shells were found to grow from 2−3 monolayers to 5−8 monolayers.[12,13] This is also not unexpected as the aging conditions here were milder than our previous work;[12,13] the upper potential limit was lowered to +1.0 from +1.2 V and above, and the experiment was carried out at room temperature, not 80 °C or higher.

EELS mapping is key for understanding how Pt is redeposited, that is, whether the nanoparticle coarsening is dominated by Ostwald ripening or coalescence? In Ostwald ripening, larger nanoparticles grow at the expense of smaller ones with the small ones eventually being consumed. In such a scenario, a single-core particle should be expected.[36,37] On the other hand, in coalescence, two or more particles merge together to form a multicore particle.[36,37] Since only Pt should be able to redeposit over this potential range, the Pt-rich shell should be much thicker in Ostwald ripening when compared to coalescence. If Ostwald ripening played major role, then the shell thickness on multicore particles should consequently be much larger than on single-core particles. However, as we determined in a statistical box plot (Supporting Information Figure 9S), no obvious difference in shell thickness between multicore and single-core nanoparticles could be observed. Therefore, we conclude that the electrochemical aging in our study is mainly dominated by coalescence.

Taking advantage of the distinctive dissolution and redeposition properties of Pt and Co, we found that coalescence played a major role in the coarsening of the particles using atomic-scale chemical mapping. However, the trajectories of the coalesced particles were still missing, which made it difficult to understand the underlying driving force(s) for this particular coarsening mechanism. To overcome this limitation, the electron tomography[17−20] of a Pt−Co nanocatalyst region, obtained at exactly the same location both before and after electrochemical aging, is shown in Figure 4. The area was chosen to be representative of a typical particle distribution and carbon support morphology (Supporting Information Figures 6S and 7S). By overlaying the reconstructions before and after the aging, we can directly visualize particle movement and coalescence (Figure 4a,b, and Supporting Information Movie 1S). It is immediately evident that most particles did not move after aging, which was confirmed by comparing the volume distribution and nearest neighbor distances (Supporting Information Figure 10S). The mean particle radius, around 3.2 nm, also did not change significantly; any changes that may have occurred were within the error of the measurement and represented no

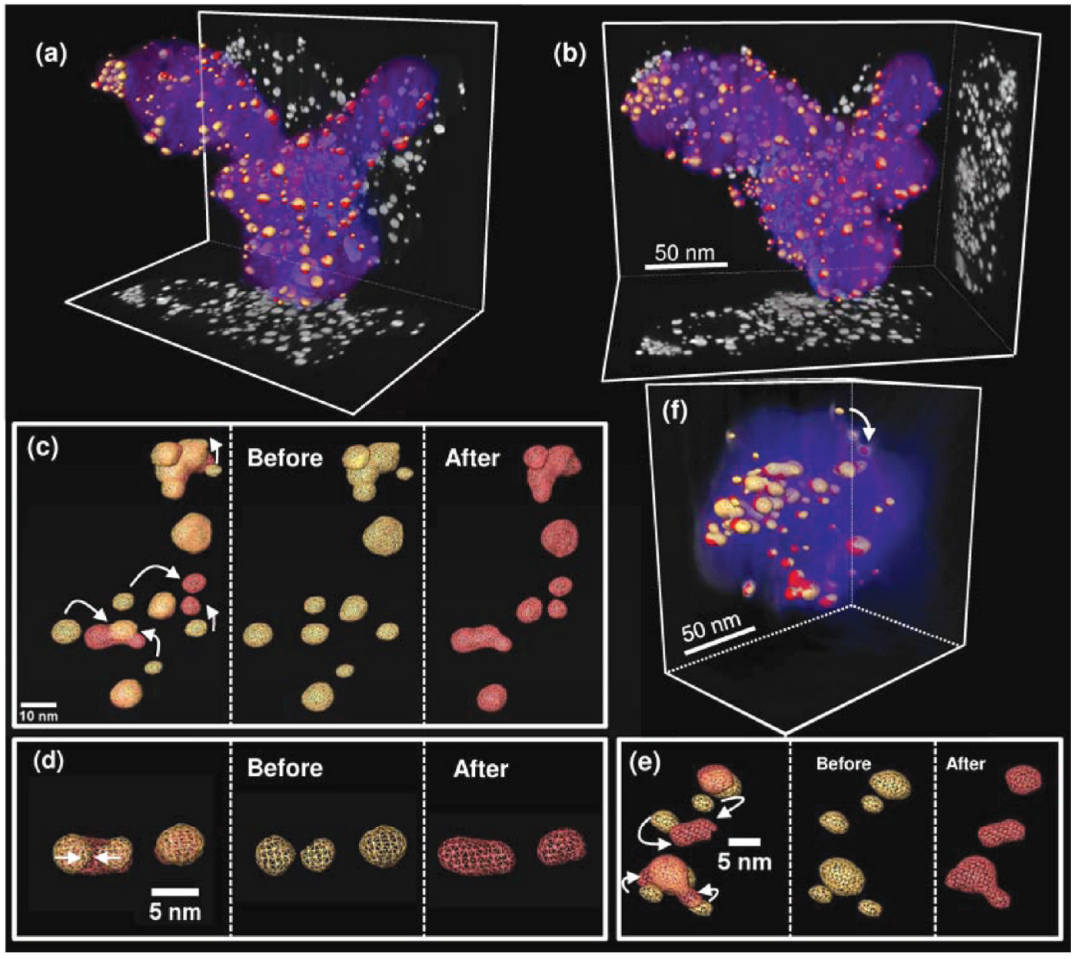

Figure 4. One-to-one correspondence of nanocatalyst particles before (gold) and after (red) electrochemical aging, which is the same color scheme used in all figures. (a) A 3D reconstruction of nanocatalyst particles, on the carbon support (violet) with projected 2D images shown at each side. (b) Alternate viewing angle. (c−e) Several instances of nanocatalyst particle coalescence and migration, with particle positions indicated by arrows. (f) One example of cropped volume from (a,b), showing how one nanocatalyst particle moves into the positive curvature (valley) from the negative curvature (summit) of the catalyst support. The arrow points out the trajectory of the particle movement. Violet shading is the carbon support.

dx.doi.org/10.1021/nl203920s | *Nano Lett.* 2012, 12, 4417−4423

more than one Pt monolayer (Supporting Information Figure 12S). The preservation of particle positions greatly facilitated accurate alignment of the reconstructions in 3D. The large set of fiduciary particles enabled an alignment fine enough to detect even small movements (1−2 nm) on the carbon support. A more dramatic example of particle migration is visualized in Figure 4f, where a nanocatalyst particle "falls" from the negative curvature (summit) into the positive curvature (valley) of the carbon support. We suspect this movement is likely driven by maximizing the contact area with the carbon support.

The electrochemical results (hydrogen adsorption regions in Figure 2a and Supporting Information Figure 3S) suggest that the ratio of {100} to {111} facets increased during the cycling. Tracking particles one-by-one, before and after electrochemical aging, also reveals the coarsening mechanisms in the system. We found that the majority of the coarsening events were caused by particle coalescence, as illustrated in Figure 4c−e. The particles were seen to both migrate and coalesce with adjacent particles. This is in contrast to Ostwald ripening, where the particles dissolve and uniformly redeposit onto larger particles nearby. After coalescence, there is a further diminution of surface area that takes place during the dissolution−redeposition process when the connection between the coalesced particles is rounded off to minimize surface energy. This is best seen in Figure 4d, where two separate particles clearly merged uniformly. Such a result is in agreement with our previously proposed particle−particle interaction between coalescence and Ostwald ripening.[12,13] It is important to note that isosurfaces can sometimes be misleading with ill-chosen thresholds. (Isosurfaces represent closed surfaces of a constant value within a volume of space; it is a set of continuous function whose points group is in 3D space). Therefore, in this study all coalescence events were verified with the volumetric reconstruction data (Supporting Information Figure 11S, Movie 2S and 3S). In Supporting Information Figures 11Sd,e, a gap seen between two particles suggests they were separate before aging, while the disappearance of such a gap confirms that the two particles were in contact with each other at the end of the cycles. This faithfully substantiates our visualization of nanoparticle coalescence in three-dimensions.

Although Ostwald ripening and coalescence might coexist during electrochemical aging, it has been predicted that each of them would dominate at different potentials.[27,38] At a higher cycling potential (i.e., in MEA with hydrogen starvation), the Pt dissolution−redeposition was so severe that larger nanoparticles consumed smaller ones quickly. On the other hand, at a lower cycling potential (i.e., our case) the migration of nanoparticles mainly took place to minimize the surface tension. One way to address the complex question would be to cycle the same nanoparticles to the potential higher than +1.4 V. However, under such conditions our assumption that the gold TEM grid was stable within the electrochemical aging ranges would no longer be valid.

Moreover, it has been reported that one of the coarsening mechanisms in Pt/Pt-alloy nanoparticle systems is carbon corrosion.[22,39,40] However, no obvious carbon degradation at a scale larger than 0.5−1.0 nm was observed in our study (Supporting Information Figures 6S and 7S), although we cannot fully rule out any atomic-scale changes that might occur on the surfaces of the carbon support. The possible explanations for the contrast with previous studies are as follow. In MEA studies, the potential cycling window can be easily altered by hydrogen starvation and fuel crossover. This can cause the potential at the cathode to be as high as +1.4 V. However, in our well-defined three-electrode electrochemical system, the control of the cycling window (+0.6 to +1.0 V) is accurate. Therefore, the kinetics of carbon corrosion in this cycling window could indeed be very slow.

In summary, we report for the first time a direct 3D visualization of nanoparticle trajectories before and after electrochemical aging based on TEM grid indexing. The growth in the Pt shell thickness and observation of coalescence in 3D could explain the decrease in electrochemically active surface area and the loss of activity of Pt−Co nanocatalysts in fuel-cell cathodes. The simplicity and rigor of the three electrode system helps to rule out many factors that could take place in the MEA (such as hydrogen starvation) and therefore establishes a direct correlation between ECSA and activity loss with the sintering behavior of nanocatalysts. The sintering processes were probed by atomic-scale chemical mapping and 3D tomography. The majority of the coarsening events were determined to be coalescence but not Ostwald ripening. These findings suggest that minimization of particle movement can potentially slow down the coarsening of particles during the electrochemical aging and will be of great assistance in the future design of electrochemically durable fuel cell nanocatalysts and supports.

■ ASSOCIATED CONTENT

Ⓢ Supporting Information

The electrochemical and TEM characterizations of nanocatalyst, before and after aging, are available. Also included are three movies of nanoparticles on the carbon support. This material is available free of charge via the Internet at http://pubs.acs.org.

■ AUTHOR INFORMATION

Corresponding Author

*E-mail: (D.A.M.) dm24@cornell.edu; (H.D.A.) hda1@cornell.edu.

Author Contributions

‖These authors contributed equally to this work.

Present address

#Materials Sciences Division, Lawrence Berkeley National Laboratory, Berkeley, CA 94720, United States.

■ ACKNOWLEDGMENTS

The Pt_3Co/C and Pt/C were synthesized by Tanaka Kikinzoku Kogyo K. K. (TKK), Japan, and was generously provided by General Motor (Honeoye Falls, NY). We thank fruitful discussions with V. Liu, F. T. Wagner, and M. F. Mathais on materials characterization. Y.Y. is grateful to J. L. Grazul, M. Thomas, H. Wang, and D. A. Finkelstein for helpful suggestion on TEM, EELS, electrochemistry, and RDE, respectively. Y.Y. thanks Z. Zou (Jimei University, China) for the assistance in art design and graphics. R.H. acknowledges support from the Center for Nanoscale Systems. J.A.M. acknowledges support from an NDSEG fellowship. This work was supported by the Department of Energy though Grant DE-FG02-87ER45298, by the Energy Materials Center at Cornell, an Energy Frontier Research Center funded by the U.S. Department of Energy, Office of Basic Energy Sciences under Award Number DE-SC0001086. This work made use of the electron microscopy facility of the Cornell Center for Materials Research (CCMR) with support from the National Science Foundation Materials

Research Science and Engineering Centers (MRSEC) program (DMR 1120296).

REFERENCES

(1) Mathias, M. F.; Makharia, R.; Gasteiger, H. A.; Conley, J. J.; Fuller, T. J.; Gittleman, C. I.; Kocha, S. S.; Miller, D. P.; Mittelsteadt, C. K.; Xie, T.; Yan, S. G.; Yu, P. T. *Electrochem. Soc. Interface* **2005**, *14*, 24−35.

(2) Stamenkovic, V. R.; Fowler, B.; Mun, B. S.; Wang, G. F.; Ross, P. N.; Lucas, C. A.; Markovic, N. M. *Science* **2007**, *315*, 493−497.

(3) Gupta, G.; Slanac, D. A.; Kumar, P.; Wiggins-Camacho, J. D.; Kim, J.; Ryoo, R.; Stevenson, K. J.; Johnston, K. P. *J. Phys. Chem. C* **2010**, *114*, 10796−10805.

(4) Mazumder, V.; Chi, M.; More, K. L.; Sun, S. *J. Am. Chem. Soc.* **2010**, *132*, 7848−7849.

(5) Zhou, Y.; Neyerlin, K.; Olson, T. S.; Pylypenko, S.; Bult, J.; Dinh, H. N.; Gennett, T.; Shao, Z.; O'Hayre, R. *Energy Environ. Sci.* **2010**, *3*, 1437−1446.

(6) Wang, C.; van der Vliet, D.; More, K. L.; Zaluzec, N. J.; Peng, S.; Sun, S.; Daimon, H.; Wang, G.; Greeley, J.; Pearson, J.; Paulikas, A. P.; Karapetrov, G.; Strmcnik, D.; Markovic, N. M.; Stamenkovic, V. R. *Nano Letters* **2010**, *11* (3), 919−926.

(7) Stamenkovic, V. R.; Mun, B. S.; Arenz, M.; Mayrhofer, K. J. J.; Lucas, C. A.; Wang, G.; Ross, P. N.; Markovic, N. M. *Nat. Mater.* **2007**, *6* (3), 241−247.

(8) Greeley, J; Stephens, I. E. L.; Bondarenko, A. S.; Johansson, T. P.; Hansen, H. A.; Jaramillo, T. F.; Rossmeisl, J; Chorkendorff, I; Nørskov, J. K. *Nature Chem.* **2009**, *1* (7), 552−556.

(9) Stanis, R. J.; Kuo, M. C.; Rickett, A. J.; Turner, J. A.; Herring, A. M. *Electrochim. Acta* **2008**, *53* (28), 8277−8286.

(10) Sugawara, S.; Maruyama, T.; Nagahara, Y.; Kocha, S. S.; Shinohra, K.; Tsujita, K.; Mitsushima, S.; Ota, K. *J. Power Sources* **2009**, *187* (2), 324−331.

(11) Chen, S.; Gasteiger, H. A.; Hayakawa, K.; Tada, T.; Shao-Horn, Y. *J. Electrochem. Soc.* **2010**, *157* (1), A82−A97.

(12) Xin, H. L.; Mundy, J. A.; Liu, Z.; Cabezas, R.; Hovden, R.; Kourkoutis, L. F.; Zhang, J.; Subramanian, N. P.; Makharia, R.; Wagner, F. T.; Muller, D. A. *Nano Letters* **2011**, DOI: 10.1021/nl203975u.

(13) Xin, H.; Mundy, J.; Cabezas, R.; Fitting-Kourkoutis, L.; Muller, D.; Liu, V.; Zhang, J.; Subramanian, N.; Makharia, R.; Wagner, F. *Microsc. Microanal.* **2010**, *16* (SupplementS2), 104−105.

(14) Shao-Horn, Y.; Sheng, W. C.; Chen, S.; Ferreira, P. J.; Holby, E. F.;
Morgan, D. *Top. Catal.* **2007**, *46* (3−4), 285−305.

(15) Liu, Z. Y.; Brady, B. K.; Carter, R. N.; Litteer, B.; Budinski, M.; Hyun, J. K.; Muller, D. A. *J. Electrochem. Soc.* **2008**, *155* (10), B979−B984.

(16) Schulenburg, H.; Schwanitz, B.; Linse, N.; Scherer, G. n. G.; Wokaun, A.; Krbanjevic, J.; Grothausmann, R.; Manke, I. *J. Phys. Chem. C* **2011**, *115* (29), 14236−14243.

(17) Xin, H. L.; Ercius, P.; Hughes, K. J.; Engstrom, J. R.; Muller, D. A. *Appl. Phys. Lett.* **2010**, *96* (22), 223108.

(18) Midgley, P. A.; Weyland, M. *Ultramicroscopy* **2003**, *96* (3−4), 413−431.

(19) Midgley, P. A.; Dunin-Borkowski, R. E. *Nat. Mater.* **2009**, *8* (4), 271−280.

(20) Li, H.; Xin, H. L.; Muller, D. A.; Estroff, L. A. *Science* **2009**, *326* (5957), 1244−1247.

(21) Hartl, K.; Hanzlik, M.; Arenz, M. *Energy Environ. Sci.* **2011**, *4* (1), 234−238.

(22) Liu, Z. Y.; Zhang, J. L.; Yu, P. T.; Zhang, J. X.; Makharia, R.; More, K. L.; Stach, E. A. *J. Electrochem. Soc.* **2010**, *157* (6), B906−B913.

(23) Mayrhofer, K. J. J.; Meier, J. C.; Ashton, S. J.; Wiberg, G. K. H.; Kraus, F.; Hanzlik, M.; Arenz, M. *Electrochem. Commun.* **2008**, *10* (8), 1144−1147.

(24) Mayrhofer, K. J. J.; Ashton, S. J.; Meier, J. C.; Wiberg, G. K. H.; Hanzlik, M.; Arenz, M. *J. Power Sources* **2008**, *185* (2), 734−739.

(25) Darling, R. M.; Meyers, J. P. *J. Electrochem. Soc.* **2003**, *150* (11), A1523−A1527.

(26) Mathias, M. F.; Makharia, R.; Gasteiger, H. A.; Conley, J. J.; Fuller, T. J.; Gittleman, C. J.; Kocha, S. S.; Miller, D. P.; Mittelsteadt, C. K.; Xie, T.; Yan, S. G.; Yu, P. T. *Electrochem. Soc. Interface* **2005**, *14* (3), 24−35.

(27) Kinoshita, K.; Lundquist, J. T.; Stonehart, P. *J. Electroanal. Chem. Interfacial Electrochem.* **1973**, *48* (2), 157−166.

(28) Strasser, P.; Koh, S.; Anniyev, T.; Greeley, J.; More, K.; Yu, C.; Liu, Z.; Kaya, S.; Nordlund, D.; Ogasawara, H.; Toney, M. F.; Nilsson, A. *Nature Chem.* **2010**, *2* (6), 454−460.

(29) Cerviño, R. M.; Triaca, W. E.; Arvia, A. J. *Electrochim. Acta* **1985**, *30* (10), 1323−1327.

(30) Frelink, T.; Visscher, W.; van Veen, J. A. R. *J. Electroanal. Chem.* **1995**, *382* (1−2), 65−72.

(31) Peuckert, M.; Yoneda, T.; Betta, R. A. D.; Boudart, M. *J. Electrochem. Soc.* **1986**, *133* (5), 944−947.

(32) Rinaldo, S. G.; Stumper, J. r.; Eikerling, M. *J. Phys. Chem. C* **2010**, *114* (13), 5773−5785.

(33) Wang, D.; Xin, H. L.; Yu, Y.; Wang, H.; Rus, E.; Muller, D. A.; Abruña, H. D. *J. Am. Chem. Soc.* **2010**, *132* (50), 17664−17666.

(34) Muller, D. A.; Kourkoutis, L. F.; Murfitt, M.; Song, J. H.; Hwang, H. Y.; Silcox, J.; Dellby, N.; Krivanek, O. L. *Science* **2008**, *319* (5866), 1073−1076.

(35) Kourkoutis, L. F.; Xin, H. L.; Higuchi, T.; Hotta, Y.; Lee, J. H.; Hikita, Y.; Schlom, D. G.; Hwang, H. Y.; Muller, D. A. *Philos. Mag.* **2010**, *90* (35−36), 4731−4749.

(36) Bowker, M. *Nat. Mater.* **2002**, *1* (4), 205−206.

(37) Campbell, C. T.; Parker, S. C.; Starr, D. E. *Science* **2002**, *298* (5594), 811−814.

(38) Adzic, R.; Büchi, F. Springer Science and Business Media: New York, 2009; p 7.

(39) Ball, S. C.; Hudson, S. L.; Thompsett, D.; Theobald, B. *J. Power Sources* **2007**, *171* (1), 18−25.

(40) Xu, F.; Wang, M. X.; Liu, Q.; Sun, H. F.; Simonson, S.; Ogbeifun, N.; Stach, E. A.; Xie, J. *J. Electrochem. Soc.* **2010**, *157* (8), B1138−B1145.